Raman and Infrared Fingerprint Spectroscopy of Peroxide-Based Explosives

JIMMIE OXLEY,* JAMES SMITH, JOSEPH BRADY, FAINA DUBNIKOVA, RONNIE KOSLOFF,* LEILA ZEIRI, and YEHUDA ZEIRI*

Chemistry Department, University of Rhode Island (URI), Kingston, Rhode Island (J.O., J.S., J.B.); Institute of Chemistry, Hebrew University, Jerusalem 91904, Israel (F.D., R.K.); Fritz Haber Institute for Molecular Dynamics, Hebrew University, Jerusalem 91904, Israel (R.K.); Department of Chemistry, Ben-Gurion University (BGU), Beer-Sheva 84105 Israel (L.Z.); Chemistry Division, NRCN, P.O. Box 9001 Beer-Sheva 84190, Israel (Y.Z.); and Department of Biomedical Engineering, Ben-Gurion University, Beer-Sheva 84105 Israel (Y.Z.)

A comparative study of the vibrational spectroscopy of peroxide-based explosives is presented. Triacetone triperoxide (TATP) and hexamethylenetriperoxide-diamine (HMTD), now commonly used by terrorists, are examined as well as other peroxide-ring structures: DADP (diacetone diperoxide); TPTP [3,3,6,6,9,9-Hexaethyl-1,2,4,5,7,8-hexaoxo-nonane (tripentanone triperoxide)]; DCypDp {6,7,13,14-Tetraoxadispiro [4.2.4.2]tetradecane (dicyclopentanone diperoxide)}; TCypDp {6,7,15,16,22,23-Hexaoxatrispiro[4.2.4.2.4.2] henicosane (tricyclopentanone triperoxide)}; DCyhDp {7,8,15,16-tetraoxadispiro [5.2.5.2] hexadecane (dicyclohexanone diperoxide)}; and TCyhTp {7,8,14,15,21,22-hexaoxatrispiro [5.2.5.2.5.2] tetracosane (tricyclohexanone triperoxide)}. Both Raman and infrared (IR) spectra were measured and compared to theoretical calculations. The calculated spectra were obtained by calculation of the harmonic frequencies of the studied compounds, at the density functional theory (DFT) B3LYP/cc-pVDZ level of theory, and by the use of scaling factors. It is found that the vibrational features related to the peroxide bonds are strongly mixed. As a result, the spectrum is congested and highly sensitive to minor changes in the molecule.

Index Headings: **Explosives; Improvised explosives; IEDs; Triacetone triperoxide; Peroxides; Remote detection; Raman spectroscopy; Infrared spectroscopy; IR spectroscopy.**

INTRODUCTION

Peroxide-based explosives have not been used extensively in civilian or military applications due to their high sensitivity to mechanical impact. Unfortunately, the ease of syntheses of some of these, particularly triacetone triperoxide (TATP), diacetone diperoxide (DADP), and hexamethylene triperoxidediamine (HMTD), from readily available chemicals makes them popular fillers for improvised explosive devices (IEDs). A number of studies have been concerned with the synthesis, structures, properties, and methods of analysis of these and other cyclic peroxides.[1–11] Sometimes they are used as the main charge, but since they are sufficiently unstable, terrorists generally only use them as the initiating explosive. These materials are white, often as innocuous looking as sugar, and unlike conventional explosives they contain no nitro groups, nor do they have metallic elements, as many initiating explosives do. Therefore, there is a great demand for analytical methodology capable of detecting these materials. Moreover, since the peroxide-based explosives have been used in a large number of suicide bombings, stand-off detection methodologies are essential.[12–16]

Technology based on spectroscopic methods has the potential to be part of a screening network to detect explosive devices based on peroxides. Two such studies have been published recently with the goal of using infrared (IR) and Raman spectroscopes to detect TATP.[17,18] Development of such methods depends on the ability to find unique spectroscopic signatures with a large cross-section. The present study is aimed at prospecting the IR and Raman spectroscopic bands. The goal is to obtain the characteristics of vibrational spectral lines with large IR or Raman intensity in a unique spectral region. It would be highly beneficial if the spectral features identified were in regions that are clear of those corresponding to atmospheric species, the so called "windows". These optical atmospheric windows exist in the following wavelength regions: 909–1333, 2083–2273, and 2381–2630 cm^{-1}. Preferably, the spectral features that will be identified should represent the family of peroxide-based explosives with the caveat that they are able to discriminate the explosives from, for example, peroxides used in various laundry detergents.

In the present investigation TATP is used as a template to identify the main spectral features of peroxide-based explosives. The method of analysis is based on comparing the experimental spectra to the results of quantum mechanical calculations. This comparison enables the assignment of the spectral features to vibrational motions. Based on this assignment we investigate the evolution of the spectral features due to chemical substitution of the side chains. This is important because most of these species have not been synthesized. In addition, these features are compared to the ones observed in other peroxide-based explosives as well as to inert peroxides.

EXPERIMENTAL TECHNIQUES

The Raman spectra presented in this study were measured in two laboratories, one at the Ben-Gurion University, BGU (in Israel), and the other at the University of Rhode Island, URI (in the USA). The Raman system at BGU comprised a Jobin-Yvon LabRam HR 800 micro-Raman system, equipped with a liquid-N_2-cooled detector. The excitation sources used in the BGU lab were a HeNe laser with an excitation wavelength of 633 nm and a Melles–Griot air-cooled Ar ion laser at 488 nm. Each excitation line has its own interference filter (for filtering out the plasma emission) and a suitable Raman notch filter (for laser light rejection). The objective used to focus the laser light was 100×. Typical Raman measurements took 1–5 minutes. The power on the sample was reduced by neutral density (ND) filters to the range of 1–100 μW to prevent photo-degradation of the samples. Most measurements were performed using the 600 grooves/mm^{-1} grating and a confocal microscope with a

Received 30 January 2008; accepted 16 May 2008.
* Author to whom correspondence should be sent. E-mail: joxley@uri.edu, ronnie@fh.huji.ac.il, yehuda@bgu.ac.il.

0003-7028/08/6208-0906$2.00/0

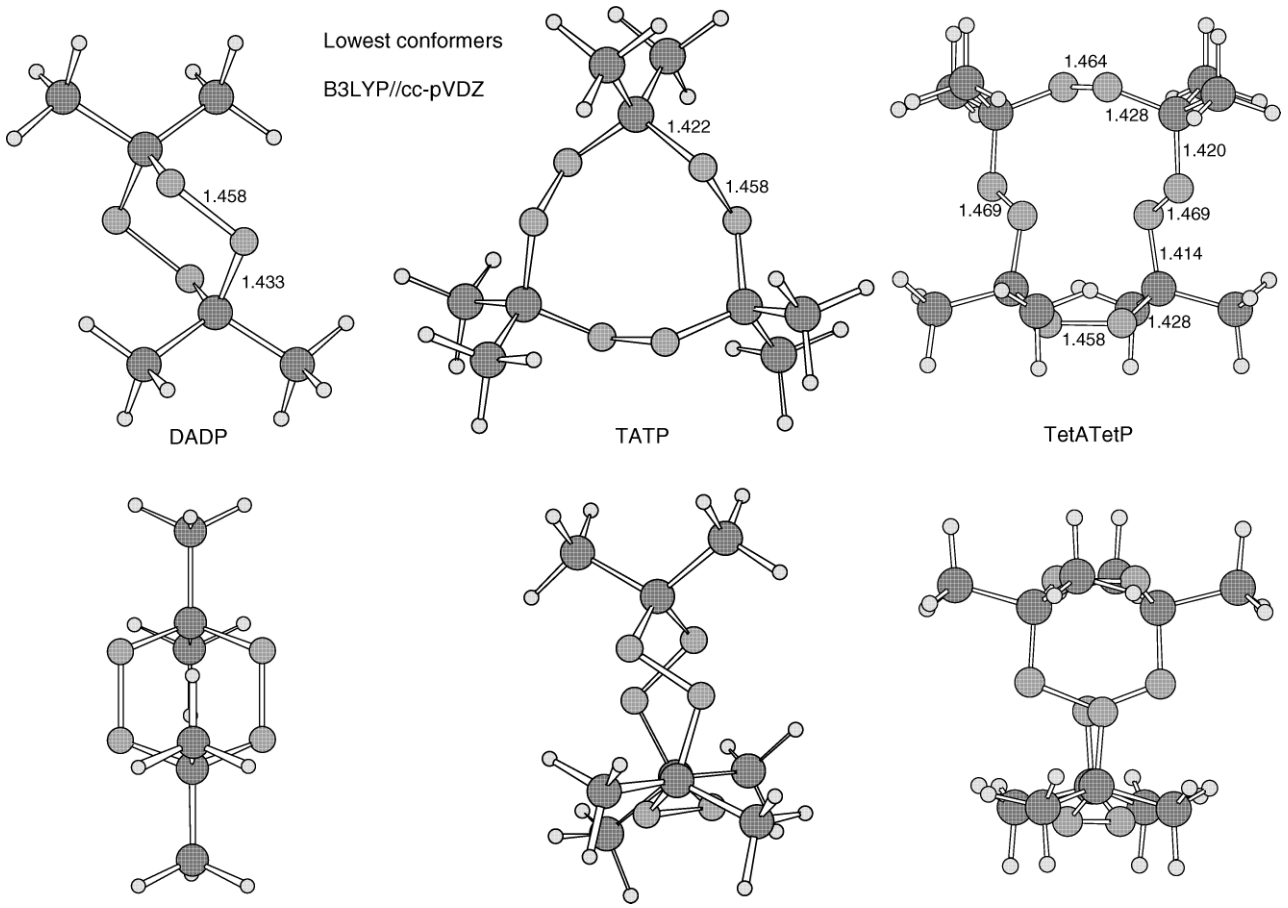

FIG. 1. (**Upper row**) Top and (**lower row**) side views of (**left**) diacetone diperoxide, (**middle**) triacetone triperoxide, and (**right**) tetraacetone tetraperoxide. All distances are in Angstroms.

100 cm^{-1} hole, giving a resolution of 4–8 cm^{-1}. Controlling sample temperature in the range 80–300 K was carried out using a Linkam unit with THMS600 stage. The TATP used for the BGU experiments was obtained from Rafael Advanced Defence Systems Ltd. as solution in acetone (1 mg/mL). Samples were prepared by deposition of 10–20 μL solutions on glass substrates. Micro-crystals of TATP were formed upon the acetone evaporation.

Raman spectra collected at URI used a Bruker Optics Senterra dispersive Raman microscope. The excitation source was a variable power (1, 10, 25, 50, 100 mW) neon laser emitting at 785 nm. The optimal aperture was found to be 25 × 1000 μm at 100 mW power with an integration time of 50 seconds and 4 co-additions. By selecting a 1200 lines/cm grating, a resolution of ~3–5 cm^{-1} was achieved at ambient temperatures. Each spectrum was collected individually in three separate regions; 80–1500 cm^{-1}, 1480–2600 cm^{-1}, and 2370–3280 cm^{-1}. TATP was synthesized in the laboratory and recrystallized from methanol and then pentane. Crystals (~1 mm square, ~1 mg in weight) were placed on a SpectRIM™ slide, which is a hydrophobic coated stainless steel substrate for Raman spectroscopy provided by Tienta Sciences.

COMPUTATIONAL METHODS

The objective of the calculations was to obtain a high degree of accuracy in geometries, binding energies, and vibrational frequencies. The calculations were carried out using the density functional theory (DFT) based method as implemented in the Gaussian 03 code package[19] with the Dunning correlation consistent polarized double ζ (cc-pVDZ) basis set.[20] Accuracy of the method was established by calculating the ground-state properties of the TATP and DADP molecules. The calculated geometries were compared to data obtained from X-ray diffraction (XRD) measurements and described previously.[7] Good agreement[7] between the calculated and experimental results is noteworthy, considering the fact that the calculation was performed on a single isolated molecule in the gas phase, while the experimental data correspond to the molecular structure in the crystalline state. This agreement suggests that the intermolecular forces in the solid phase are too weak to cause any significant alteration of the molecular geometry. Figure 1 shows an example of the calculated structure of peroxide-based explosives. Top and side views of three explosives are shown: DADP (left structures), TATP (middle structures), and tetraacetone tetraperoxide, TetATetP (right structures). The three structures describe the ground-state lowest energy conformations of these stable molecules.

Once the structure has been determined, the normal modes of the molecules are calculated, using the standard suit in Gaussian 03 to determine the harmonic frequencies. In a few cases, results were compared to data obtained by other electronic structure codes such as GAMESS-USA (version December 2002)[21] and Q-Chem (version 2.1).[22] All methods gave approximately the same harmonic frequencies within an

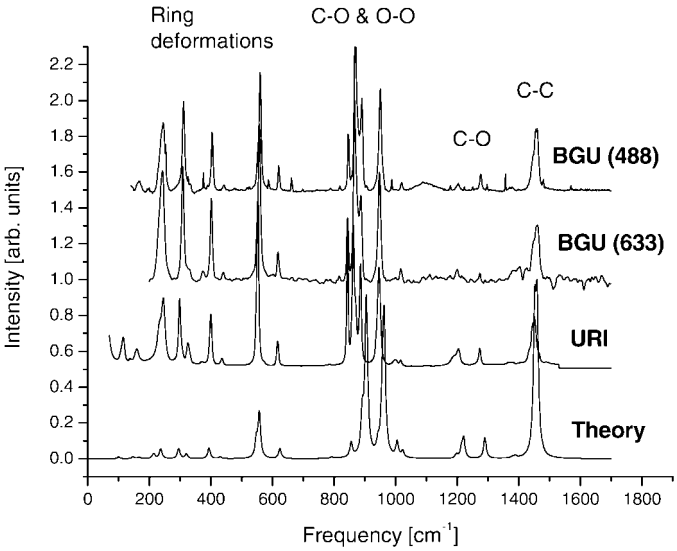

FIG. 2. Raman spectra of TATP. The calculated data is compared with three different experimental measurements.

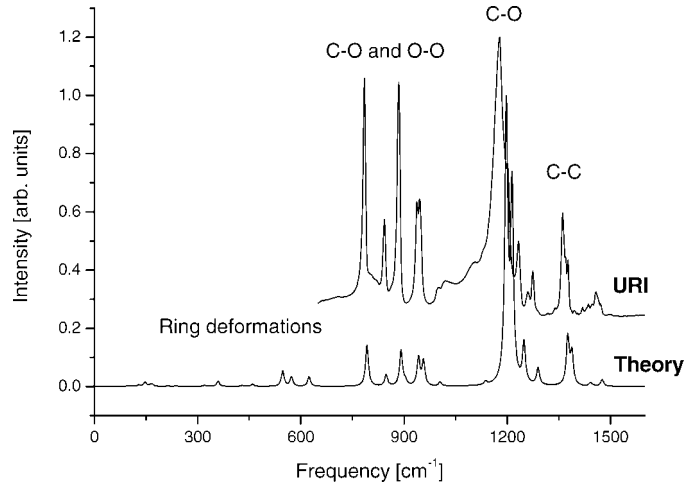

FIG. 3. Infrared spectra of TATP. The calculated data is compared with the experimental measurements.

accuracy of a few wavenumbers (cm^{-1}). Vibrational frequencies were also calculated using two approximations of the hybrid exchange-correlation function, the B3LYP[23] and the B-971[24] (both available in Gaussian 03). The vibration frequencies obtained were very close to each other with differences in the range of 0.2–7 cm^{-1}. Hence, all the results described below correspond to Gaussian 03 simulation employing the B3LYP/cc-pVDZ level of theory.

The spectroscopic signatures of interest are mostly imbedded in the structure of the molecular skeleton. As a result, there are strong anharmonic effects that are able to shift some spectral features. This shift is estimated to be in the range of ~30–40 cm^{-1}. Thus, anharmonic corrections were obtained using the vibrational self-consistent field[25] (VSCF) method.[26] In the present study, harmonic frequencies are used for the assignment, and spectral regions where anharmonic corrections are expected to be significant are noted. Comparison between the outcome in the calculations and the experiment reveals that, in general, the harmonic approximation is sufficient to assign the spectrum. In particular, the harmonic approximation is able to follow the spectral shift due to substitution, thus allowing assignment of spectral features to peroxides that have not been isolated.

The differences in relative intensities and peak positions between the calculated and measured spectra are attributed to the approximations used in the calculations. The two main approximations employed are (1) overall neglect of anharmonicity, and (2) an approximate description of electron correlation due to the use of an incomplete basis set. The use of the harmonic approximation together with neglect of coupling between the different vibrational modes (overtone bands) in the calculation leads to shifts in the calculated frequencies of 5 to 30 cm^{-1} compared to the experimental values. The coupling among the vibrational modes may give rise to bands associated with overtones that are missing in the calculated spectrum. There were a number of attempts to correct these inaccuracies in the calculated frequencies. The approach proposed by Pople et al.[27] suggested multiplying all frequencies by a common factor of 0.8929 since calculated frequencies were over-estimated by about 12%. The scaling factor was changed to 0.99 for DFT calculations of frequencies by Rauhut and Pulay.[28] More recently, Sinha et al.[29] performed extensive calculations and compared the accuracy in harmonic frequency determination by three levels of calculations and different basis sets. The most accepted scaling factor was suggested by Scott and Radom.[30] Their value has been implemented in the Gaussian 03 B3LYP/6-31G(d) calculation and it is 0.9614. The contribution of anharmonicity can be estimated from an analysis of the temperature-dependent variation of the vibrational spectral features.[31] All the calculated spectra in this study are obtained from B3LYP/cc-pVDZ frequencies and dipole strengths using Lorentzian band shapes ($\gamma = 1.0$ cm^{-1}).

THE INFRARED AND RAMAN SPECTRA OF TATP

The vibrational spectra, Raman and IR, of TATP will be used in this work as a typical spectrum of peroxide-based explosives. The spectral features associated with peroxide and C–O bonds of TATP are similar to those of O–O and C–O bonds in other organic molecules. However, the detailed features of the vibrational spectra will be determined by the actual composition and structure of the investigated molecule. The Raman and IR spectra of TATP are shown in Figs. 2 and 3, respectively. The Raman spectra in Fig. 2 correspond to TATP as obtained in the calculations, in URI (at room temperature) and in BGU (at 273 °C) at two different excitation wavelengths (488 and 633 nm), while in Fig. 3 we compare the experimental (URI) and theoretical IR spectra for TATP. It should be noted that there is a major difference between the procedures used to measure the Raman spectra in the two laboratories. In URI the spectrum was obtained using TATP crystals synthesized in the laboratory (~1 mm square, about 1 mg in weight). In contrast, the measurements at BGU were performed on a thin film of TATP on glass, obtained by deposition of 20 μL of TATP solution in acetone (1 mg/mL) and evaporation of the solvent. The TATP film obtained in this procedure is constituted of very small crystals; hence, the relative intensities and line widths are different than those observed in URI using much larger crystals.

The measurements at BGU were difficult due to instability of

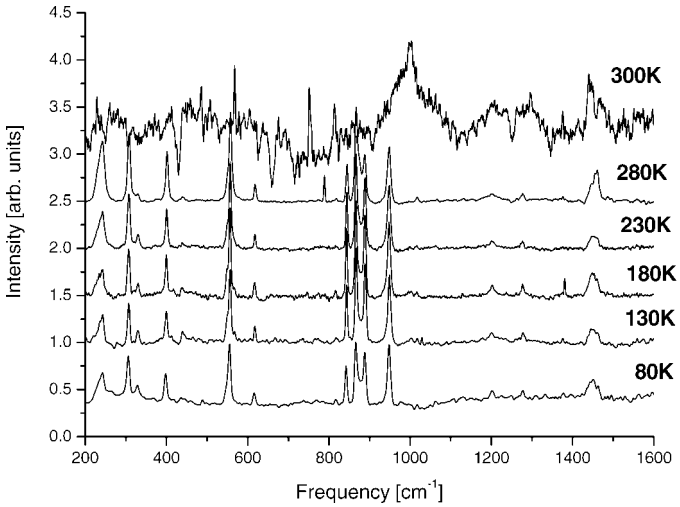

FIG. 4. Temperature dependence of the TATP Raman spectra (not including the C–H stretching and bending modes near 3300 cm^{-1}).

the sample at room temperature. The spectra were very strong for short times but disappeared during the collection period. Cooling of the samples to temperatures lower than 280 K yielded stable spectra that could be measured without any difficulty. The spectra obtained at the lower temperatures were very similar to the unstable spectra observed at room temperature.

Agreement between the measured and calculated spectra is reasonable. Inspection of the Raman spectra (Fig. 2) shows that the Raman peaks are nearly independent of the excitation wavelength and of the crystal size. The features at 1460 cm^{-1} correspond to the C–C stretching mode, and there is good agreement of the calculated and measured data. The weak feature between 1200–1300 cm^{-1} corresponds to the peroxide C–O ring stretches. These are the strongest features in the IR spectra (Fig. 3). The strongest features in the Raman spectra are obtained in the range 900–1000 cm,$^{-1}$ and they represent a combination of the ring O–O and C–O stretching modes. The corresponding calculated peaks are blue shifted relative to the measured peaks. The collection of peaks between 200–600 cm^{-1} corresponds to ring deformation modes. As seen in Fig. 2, some of these features exhibit very high intensities. The corresponding region in the calculated spectrum shows that the frequencies are slightly blue shifted and the intensities are reduced compared to the experimental data. In addition, there are, in this spectral region, some small differences between the Raman spectra obtained using the two different excitation sources (an extra peak at about 680 cm^{-1} using the 488 nm light).

Inspection of Fig. 3 shows strong IR absorption at the peroxide O–O and C–O stretching modes in the range 900–1000 cm^{-1}. It might be expected that the peroxide O–O stretch modes be absent in the IR spectrum. Their strong appearance is an indication of strong mixing with the C–O modes. Comparison of the calculated peaks and the measured ones in this region shows that the theoretical spectrum is red shifted relative to the experimental data. This red shift is associated with mixing among the normal modes of the molecules.

We have measured the Raman spectra of TATP at different temperatures in the range 80–298 K. Typical results of these experiments are presented in Fig. 4. The spectra measured at 300 K are very noisy due to the instability of the sample at this temperature (Fig. 4). Reduction of the sample temperature to 280 K or below yields strong and stable spectra. Careful examination of these results shows that there are marked variations in the relative intensities of some of the spectral features. In addition, for some of the vibrational bands there are small (1–3 cm^{-1}) shifts in the peak position as well as in its width at half maximum. These changes are observed when temperature is increased from 80 K to room temperature. These variations can be related to changes in the relative intensities of

TABLE I. TATP calculated (at B3LYP/cc-pVDZ level of theory) harmonic frequencies (cm^{-1}), IR intensities (km/mole), Raman scattering activities (A^4/AMU), and frequencies. Table includes only the frequencies (all of them) that are concerned with O–O and C–O vibrations.

	Frequency	IR intensity	Raman activity	Description		Frequency	IR intensity	Raman activity	Description
ν_1	99.2	0.7	0.4	O–O–C–Me tors tangent to ring	ν_{32}	792.6	28.6	0.3	O–C–O sym str and Me–C–Me sym str
ν_2	100.1	0.6	0.4	O–O–C–Me tors	ν_{33}	848.1	15.4	0.0	Collective O–C–O asym str
ν_3	129.1	1.9	0.0	Collective O–O–C–Me tors	ν_{34}	855.5	0.0	7.4	Collective O–C–O and Me–C–Me sym str
ν_4	147.0	2.8	0.4	O–O–C–Me tors and Me twist asynch.	ν_{35}	891.2	24.7	10.1	O–C–O and Me–C–Me asym str, Me–C–O sym str
ν_5	147.6	3.2	0.5	O–O–C–Me tors and Me twist asynch.	ν_{36}	891.8	24.7	10.1	O–C–O and Me–C–Me sym str, Me–C–O asym str
ν_{13}	236.4	0.4	2.5	C–O–O–C shear	ν_{37}	903.6	3.1	32.1	O–O str asynch and Me rock asynch
ν_{14}	237.3	0.4	2.5	C–O–O–C shear	ν_{38}	904.6	3.0	32.8	O–O str asynch and Me rock synch
ν_{16}	296.3	0.3	0.0	Collective bending	ν_{39}	906.6	0.1	19.9	O–O str synch Me–C–Me sym str and Me rock synch
ν_{21}	393.7	0.0	5.4	Ring breathing	ν_{43}	956.3	17.9	13.3	Me–C–Me str, O–C–O sym str
ν_{22}	429.1	0.6	0.4	O–C–Me scis	ν_{44}	957.1	16.1	12.8	Me–C–Me and O–C–O sym str
ν_{23}	430.1	0.7	0.4	O–C–Me scis	ν_{45}	962.7	0.0	66.2	Collective O–O and C–O str
ν_{25}	547.2	10.6	4.2	O–C–Me scis and Me–C–Me rock	ν_{48}	1022.8	0.0	3.3	O–C–O sym str
ν_{26}	547.4	10.4	4.2	O–C–Me scis and Me–C–Me rock	ν_{49}	1137.2	4.6	0.0	O–C–O asym str
ν_{27}	557.1	0.0	22.8	Collective O–C–O scis	ν_{50}	1197.4	187.8	1.0	O–C–O and Me–C–Me asym str, Me–C–O sym str
ν_{28}	572.9	13.0	0.0	Collective C–C–O scis	ν_{51}	1197.6	192.6	1.0	O–C–O and Me–C–Me asym str, Me–C–O sym str
ν_{29}	623.8	6.6	2.5	O–C–O scis asynch	ν_{52}	1213.9	131.5	2.4	O–C–O and Me–C–Me sym str
ν_{30}	624.1	6.6	2.5	O–C–O scis asynch	ν_{53}	1214.0	131.4	2.4	O–C–O and Me–C–Me sym str
ν_{31}	792.1	28.6	0.3	O–C–O sym str and Me–C–Me sym str	ν_{54}	1220.9	0.0	9.8	Collective O–C–O and Me–C–Me sym str

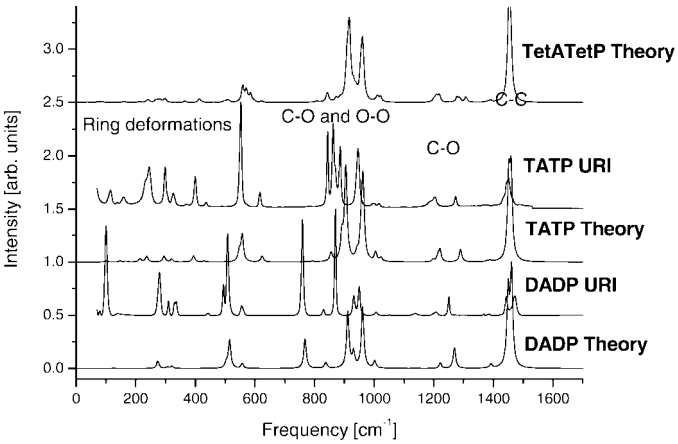

FIG. 5. Raman spectra of DADP and TATP as well as calculated spectra of DADP, TATP, and TetATetP.

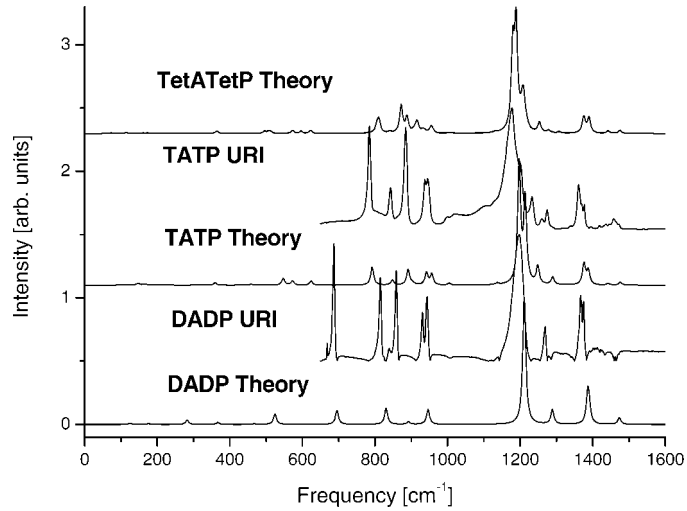

FIG. 6. Infrared spectra of DADP and TATP as well as calculated spectra of DADP, TATP, and TetATetP.

the different frequencies in the band. The Raman peaks of TATP show small temperature dependence even for the high frequency modes. This is the result of the ring structure that induces anharmonic mixing of high frequency modes with low frequency ones. Presently we are investigating different procedures to include both anharmonicity and mode coupling into the calculated spectrum.[26]

Table I summarizes the calculated assigned fingerprint spectral features of TATP. The strongest Raman line is ν_{45} near 960 cm^{-1} associated with the collective O–O stretch, along with the combination O–O stretch lines ν_{37} to ν_{39} near 900 cm^{-1}. The IR signature of these lines is much weaker.

Dependence of Vibrational Modes on Ring Size. Figure 5 displays the calculated Raman spectra of DADP, TATP, and TetATetP compared with the measured spectra for DADP and TATP, while Fig. 6 displays the corresponding IR spectra. Comparing the ring stretch modes in the Raman spectra shows that, in general, the smaller the ring, the better separated the spectral features. For example, the very strong and well-resolved peak at 786 cm^{-1} in DADP (corresponding to O–C–O and O–C-methyl stretching modes) shifts to the blue and collapses with the ring modes for TATP and TetATetP. A similar phenomenon is observed in the IR spectra (Fig. 6). Another change in the spectra when the molecular ring is enlarged is associated with the ring deformation features in the range of 200–600 cm^{-1}. Increase in the ring size results in the observation of more peaks at altered frequencies. Comparison of the calculated and measured Raman and IR spectra shows that in DADP the ring modes are mixed, and hence, the experimental data is blue shifted relative to the calculation. Again, in the low frequency region (200–600 cm^{-1}), the calculation underestimates the intensities of the deformation

TABLE II. DADP calculated (at B3LYP/cc-pVDZ level of theory) harmonic frequencies (cm^{-1}), IR intensities (km/mole), Raman scattering activities (A^4/AMU), and frequencies. Table includes only the frequencies (all of them) that are concerned with O–O and C–O vibrations.

	Frequency	IR intensity	Raman activity	Description		Frequency	IR intensity	Raman activity	Description
ν_7	274.0	0.0	0.7	O–O–C–Me tors tangent to ring	ν_{22}	837.5	0.0	3.0	O–C–O asym scis synch and O–C–Me asym scis synch
ν_8	282.4	9.1	0.0	O–O–C–Me tors asynch	ν_{23}	892.4	5.4	0.0	O–O str asynch
ν_9	305.6	0.0	0.8	O–O–C–Me tors synch	ν_{24}	911.5	0.0	28.6	O–O str synch O–C–Me asym str asynch
ν_{12}	429.1	0.0	0.1	O–C–Me scis asynch	ν_{25}	930.9	0.0	7.7	O–O–C sym str synch and Me–C–Me asym str asynch
ν_{13}	467.2	1.4	0.0	O–C–Me scis synch	ν_{27}	946.5	31.0	0.0	O–C–O str async and O–C–Me asym str synch
ν_{14}	502.0	0.0	2.3	O–O–C–O shear	ν_{28}	961.2	0.0	30.9	O–O str synch and O–C–O sym str asynch and O–C–Me asym str asynch
ν_{15}	514.7	0.0	14.4	C–O–O–C shear	ν_{31}	1137.8	0.0	0.2	O–C–O asym str asynch and O–C–Me asym str asynch
ν_{16}	524.6	21.5	0.0	O–O–C–O tors	ν_{32}	1210.5	76.7	0.0	O–C–O asym str synch and O–C–Me asym str synch
ν_{17}	557.1	0.0	2.4	O–C–O sym scis collective	ν_{33}	1212.0	191.4	0.0	O–C–O sym str asynch and O–C–Me asym str synch
ν_{18}	695.4	28.7	0.0	O–C–O sym scis asynch and O–C–Me sym scis synch	ν_{34}	1221.9	0.0	2.8	O–C–O sym str synch and O–C–Me asym str asynch
ν_{19}	786.0	0.0	15.0	O–C–O sym scis synch and O–C–Me sym scis synch	ν_{35}	1269.4	0.0	10.6	O–C–Me asym str asynch and Me–C–Me asym str asynch
ν_{20}	830.7	32.7	0.0	O–C–O asym scis synch and O–C–Me asym scis synch	ν_{36}	1289.0	30.0	0.0	O–C–Me asym str synch and Me–C–Me asym str synch
ν_{21}	834.8	0.7	0.0	O–C–O sym scis asynch					

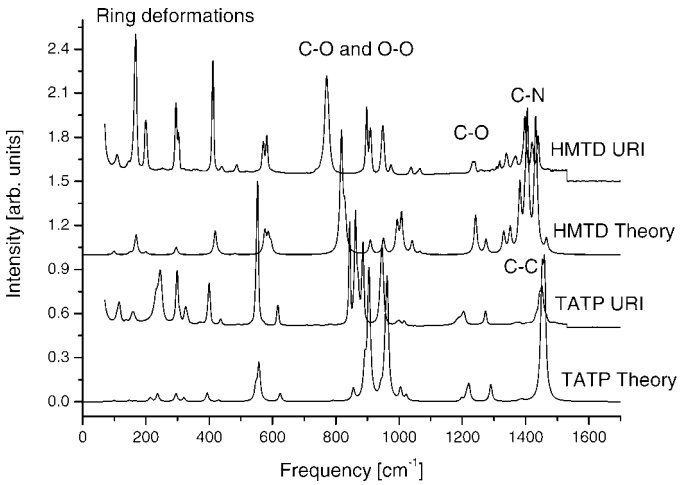

FIG. 7. Raman spectra of TATP and HMTD.

modes. However, it is clear that increase in the ring size leads to more complicated deformation structures in both Raman and IR spectra (Figs. 5 and 6). Table II shows that in DADP the main O–O stretch at 962 cm^{-1} retains the same position as in TATP. The splitting of the combinations around 910 cm^{-1} is, as expected, less pronounced and shifted slightly to the blue relative to the value obtained for TATP.

Dependence of Vibrational Modes on Molecular Skeleton Shape. To study the relationship between the shape of the molecular skeleton and the vibrational features, we compare the experimental and calculated spectra for TATP and HMTD. These two molecules possess very different skeleton shapes that "hold" the peroxide bonds together. The experimental and calculated Raman spectra for both molecules are presented in Fig. 7, while Fig. 8 displays the corresponding IR spectra. The noticeable feature in the Raman spectra (Fig. 7) is the strong peroxide O–O stretch in HMTD at approximately 800 cm^{-1}, which is red shifted relative to the calculated peak (all relevant vibrational frequencies for HMTD are summarized in Table III). The many features observed in the range 900–1100 cm^{-1} correspond to additional peroxide O–O and C–O stretches. These peroxide-related peaks in HMTD span a much larger region as compared to TATP. This is due to a more complex integrated ring structure. Inspection of the HMTD IR spectrum (Fig. 8) shows that the strongest feature is at 770 cm^{-1}. The theoretical calculation does not show this feature; however, the peaks at higher frequencies (830 and 950 cm^{-1}) are associated with O–O stretch modes.

TABLE III. HMTD calculated (at B3LYP/cc-pVDZ level of theory) harmonic frequencies (cm^{-1}), IR intensities (km/mole), Raman scattering activities (A^4/AMU), and frequencies. Table includes only the frequencies (all of them) that are concerned with O–O and C–O vibrations.

	Frequency	IR intensity	Raman activity	Description
ν_{11}	419.0	0.0	0.0	Ring breath
ν_{19}	586.5	0.1	5.2	Ring stretching
ν_{22}	817.6	0.0	35.4	O–O str (3 synch)
ν_{23}	828.7	2.7	5.4	O–O str (2 synch, 1 asynch)
ν_{24}	829.0	2.8	5.4	O–O str (2 synch)
ν_{27}	950.4	3.4	2.3	C–O str (2 pairs synch, 1 pair asynch)
ν_{28}	950.8	3.3	2.3	C–O str (2 pairs synch)
ν_{29}	993.5	27.1	4.5	O–O str (2 asynch) and C–O str (2 pairs asynch)
ν_{30}	994.0	3.9	4.5	O–O str (2 asynch) and C–O str (2 pairs synch, 1 pair asynch)
ν_{32}	1007.8	15.2	10.7	O–O str (3 synch) and C–O str (3 pairs synch)
ν_{33}	1033.5	165.6	0.0	C–O str (3 pairs synch)
ν_{38}	1081.9	0.0	0.2	C–O str (3 pairs synch)

Dependence of Vibrational Modes on Substitution in TATP. Upon substitution of the methyl groups in TATP, the spectral feature associated with the ring motion change significantly. Two types of substitutions were examined in this study. The first consists of the replacement of one or both methyl groups, on all three ring carbons, by either hydrogen atoms or ethyl groups. The second family of substitutions consists of replacement of the two methyl groups, on each ring carbon, by a cyclic hydrocarbon: cyclobutanone, cyclopentanone, and cyclohexanone. According to the calculations, all these substituted TATP species are stable molecules. However, it is not clear whether these substitutions will lead to the precipitation of stable crystalline forms of these compounds. A comparison of the calculated structure of tri-cyclohaxanon-

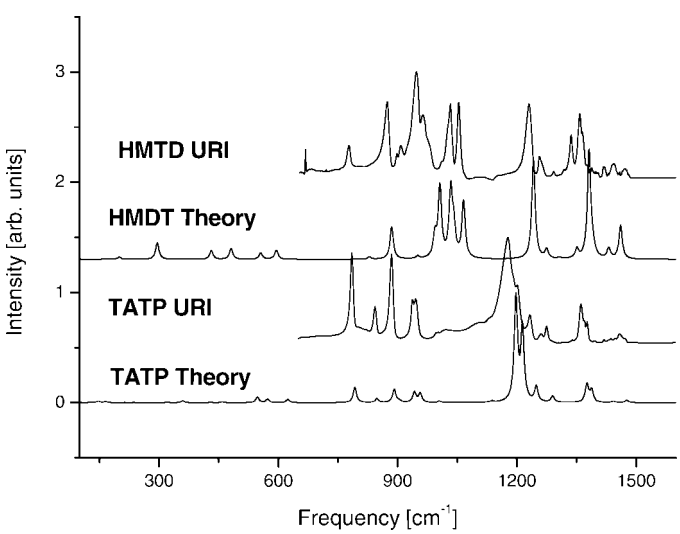

FIG. 8. Infrared spectra of TATP and HMTD.

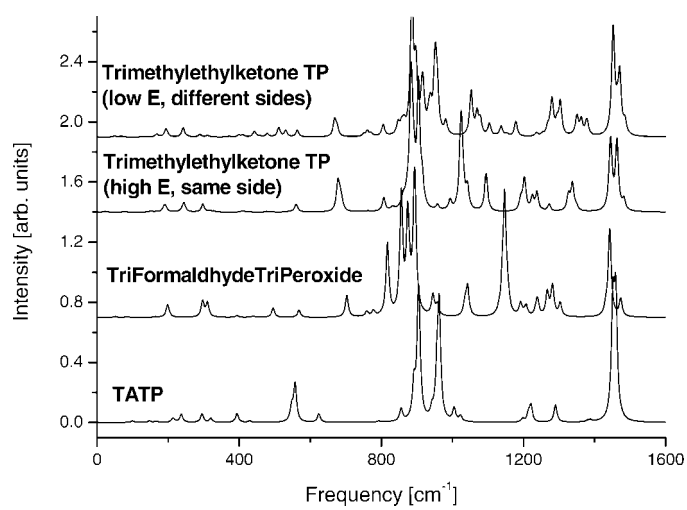

FIG. 9. Comparison of calculated Raman spectra for H and C_2H_5 substitutions in TATP.

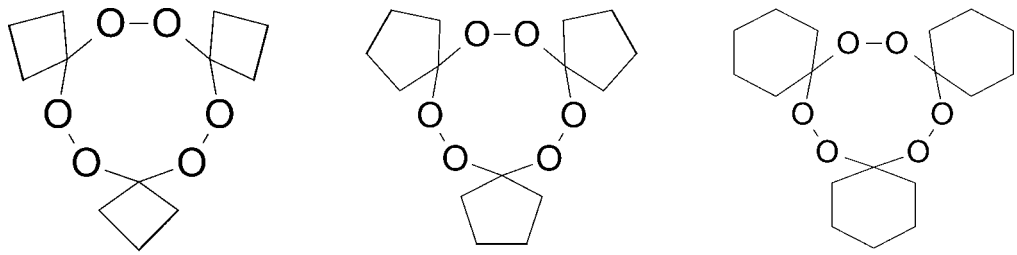

FIG. 10. Structure of cyclo-hydrocarbone substituted TATP.

triperoxide with the experimental data obtained from X-ray diffraction measurements[11] shows good agreement, indicating the reasonable reliability of the calculated data.

Figure 9 shows a comparison of calculated Raman spectra for the first family of substitutions, one or both methyl groups replaced by H atoms or ethyl groups. Comparison of the results for TATP and triformaldehyde triperoxide (TFTP) shows that substitution of the methyl groups by hydrogens leads to a separation between the peroxide O–O and C–O stretch modes. The substitution of methyl groups by ethyl groups causes additional mixing between the C–C and C–O stretch modes, hence, the appearance of new peaks in the spectra. The features associated with the ring deformation, 200–600 cm,$^{-1}$ were not much affected by the substitution of methyl groups.

Figure 10 shows the structure of three TATP molecules where the methyl groups were replaced by cyclo-hydrocarbons. Figure 11 shows a comparison of calculated Raman spectra for the family of the three substituted TATP molecules shown in Fig. 10. The Raman spectra of all the substituted molecules become much more complicated, with many additional peaks. These additional features are related to the strong mixing among all the stretch modes in the molecule. Again, the region associated with the ring deformation modes undergoes only minor changes upon substitution. The corresponding IR spectra of these substituted molecules are presented in the accompanying material. Similar behavior is observed for substituted DADP according to our calculations, namely, substitution of side chains causes spectral congestion to a point where it becomes un-assignable.

THE USE OF PEROXIDE-BASED EXPLOSIVE VIBRATIONAL SPECTRA FOR DETECTION

Like any molecule, each peroxide-based explosive has a unique splitting pattern of vibrational modes that could be employed in a high resolution detection scheme. In this family of explosives the "chromophore groups" consist mainly of the peroxide C–O and O–O bonds. However, the vibrational modes associated with these chromophores are part of a larger ring structure that includes, in addition to the chromophores, various side groups. As a result, there is strong mixing among the different modes that leads to a highly congested spectrum. Due to the strong mixing, the spectrum is also sensitive to substitutions of the side chains in the molecules. These sensitivities lead to marked changes in the spectra of the various systems, as demonstrated above. This is in contrast to military explosives in which the pendent nitro and amine groups can serve as the main chromophores.

The common use of peroxides in the detergent industry causes a practical complication in the use of vibrational spectroscopy as a tool for peroxide-based explosives identification. We interviewed manufacturers of detergents in Israel, and the conclusion of these interviews was that a wide variety of peroxides are used in different amounts and most of them are proprietary, meaning that exact formulations published on the packages are suspect. Nevertheless, typical peroxides include NaO_2COOH, peracetic acid [$CH_3CO(OOH)$], and propaneperoxoic acid $CH_3CH_2CO(OOH)$. The relevant calculated Raman and IR vibrational frequencies of these three peroxides are described in Table IV. Figure 12 compares the calculated Raman spectra of TATP to that of calculated and measured spectra of sodium percarbonate (NaO_2COOH), one of the common additives in the detergent industry, as well as to the measured Raman spectra of a common detergent used in Israel (named Percival, no ingredient information available). The commercial detergent consists of 1 to 2 mm diameter white and blue particles. The Raman spectrum of the blue particles could not be measured due to their very strong fluorescence. The morphology of the white particles suggested that they consist of two types of crystalline material marked in Fig. 12 as detergent-1 and detergent-2. The C–O and O–O modes associated with the peroxide bonds are located in TATP in the range 900–1050 cm^{-1} and in a similar region in the case of sodium percarbonate. The experimental data indicates that for sodium percarbonate these peroxide modes are red shifted to

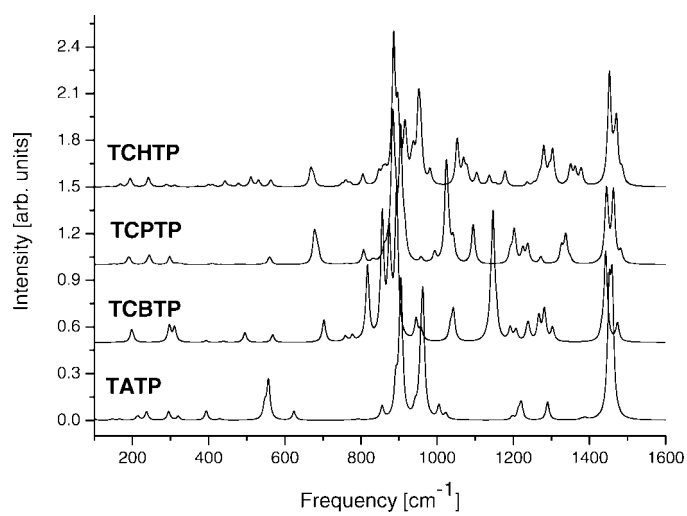

FIG. 11. Comparison of calculated Raman spectra for methyl substitution in TATP by cyclo-hydrocarbons (TCBTP: tricyclobutanone triperoxide; TCPTP: tricyclopentanone triperoxide; and TCHTP: tricyclohexanone triperoxide).

TABLE IV. Calculated (at B3LYP/cc-pVDZ level of theory) harmonic frequencies (cm^{-1}), IR intensities (km/mole), Raman scattering activities (A^4/AMU) and frequencies. Tables presented for five different peroxides used in the detergent industry.

	Frequency	IR intensity	Raman activity		Frequency	IR intensity	Raman activity
			Sodium percarbonate $Na_2^+[O_2COO]^{2-}$				
1	66.8	0.4	0.4	9	590.7	2.9	8.7
2	122.1	32.5	1.0	10	726.4	9.7	5.6
3	180.7	11.1	1.7	11	795.1	29.2	0.1
4	194.4	7.6	1.8	12	901.6	24.3	4.4
5	269.1	49.1	2.6	13	1038.6	20.8	9.1
6	343.0	52.5	7.0	14	1402.0	480.1	107.1
7	375.9	8.4	0.9	15	1560.1	661.4	4.8
8	476.7	25.6	20.5				
			$[O_2COOH]^-$				
1	199.9	0.6	0.1	7	865.5	170.7	3.6
2	393.3	9.6	1.9	8	909.9	9.3	20.6
3	542.2	0.7	4.2	9	1293.5	202.4	11.2
4	713.7	22.5	2.7	10	1534.6	272.7	10.0
5	716.9	3.2	7.0	11	1845.5	402.9	2.0
6	817.2	73.9	1.1	12	3107.0	259.1	15.0
			$[O_2COO]^{2-}$				
1	167.5	6.1	0.2	6	851.6	31.7	10.1
2	301.0	5.0	3.5	7	966.2	34.8	5.1
3	526.8	0.5	7.4	8	1328.1	526.6	6.0
4	682.1	5.3	3.6	9	1659.2	501.3	1.3
5	818.9	21.2	0.0				
			Propaneperoxoic acid 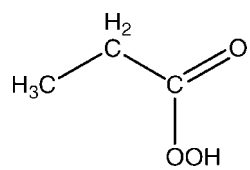				
1	42.6	0.1	0.4	16	1202.0	154.9	2.1
2	174.7	0.0	1.1	17	1276.5	16.1	4.9
3	208.8	0.1	0.1	18	1375.4	32.7	0.2
4	266.8	0.7	0.2	19	1398.0	2.2	1.7
5	355.7	29.5	0.4	20	1441.2	7.0	15.3
6	436.9	7.2	4.4	21	1465.9	7.4	15.3
7	483.2	68.0	3.5	22	1478.3	1.3	6.7
8	611.3	21.4	3.3	23	1492.8	148.9	7.1
9	703.5	6.8	2.6	24	1800.9	171.2	8.1
10	804.2	12.4	0.4	25	3038.9	6.3	122.8
11	918.9	24.8	10.5	26	3048.0	20.6	118.7
12	934.0	1.8	5.0	27	3097.5	3.2	99.2
13	1027.4	2.8	3.8	28	3122.2	19.4	69.0
14	1085.2	10.6	7.3	29	3136.7	13.4	41.1
15	1092.1	2.5	1.8	30	3411.4	80.2	26.3
			Peracetic acid 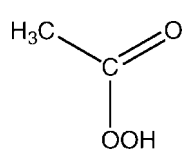				
1	59.9	131.5	5.4	12	1231.7	145.3	1.0
2	167.9	0.8	0.1	13	1374.9	40.2	2.8
3	180.4	1.7	0.1	14	1405.8	169.2	12.2
4	318.3	6.4	1.3	15	1435.0	1.7	8.6
5	486.7	6.3	0.8	16	1443.7	7.7	10.7
6	556.6	5.1	5.4	17	1861.9	244.6	13.4
7	562.0	3.9	0.8	18	3061.7	0.6	120.3
8	804.1	24.1	10.0	19	3134.0	1.8	54.3
9	948.6	2.1	17.0	20	3176.8	2.9	58.9
10	995.5	26.8	1.2	21	3735.1	79.8	105.5
11	1047.8	8.2	0.1				

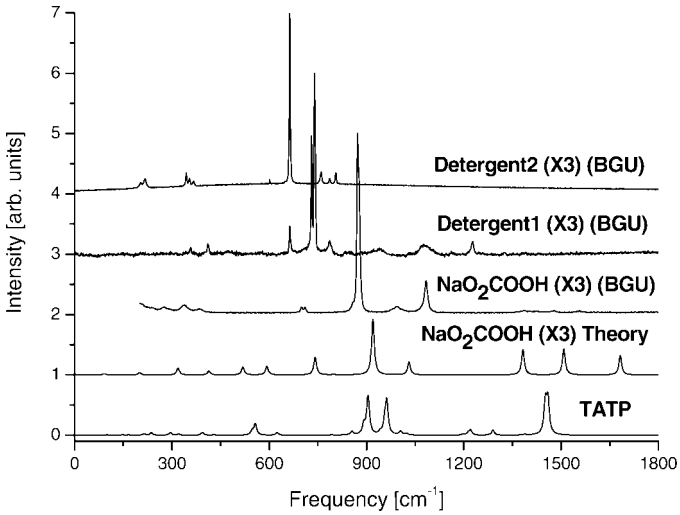

FIG. 12. Comparison of calculated and measured Raman spectra of TATP and peroxides used in detergents as well as common detergents.

the region of 850–1100 cm^{-1}. The Raman spectra obtained for the commercial detergent indicates that the modes associated with the peroxide bond are either shifted farther to the red (to the region of 650–800 cm^{-1}) or are too weak to be observed. The data shown in Fig. 12 indicated that detergent remaining may obscure peroxide associated vibrational modes of the explosive.

The data described in this study indicates that there are no unique spectral features by which peroxide-based explosives can be detected. It is clear that the detailed structure of the molecule has a large influence on its vibrational spectrum. Any modification in the skeleton or in side chains may lead to marked changes in the spectral features. This was found to be true for both Raman and IR spectra. As a result, a remote detection scheme that will be based on a limited spectral region will be difficult to use in identification of explosives with high enough confidence due to substantial errors that can be introduced by impurities in the material and interference with the peroxide-containing compounds. To obtain a more reliable detection of peroxide-based explosives, it seems that one will need to use a very broad spectral region that includes many spectral features of the detected molecule. Even so, explosive identification may be suspect since small modifications can lead to a different spectrum.

CONCLUSION

This study was devoted to a comparative investigation of measured and calculated vibrational spectroscopy of peroxide-based explosives. The common chromophore in all these molecules is the peroxide O–O and C–O bonds. These bonds are part of the molecular skeleton. As a result, the vibrational modes are strongly mixed. This vibrational mixing makes the harmonic approximation, used to calculate the spectra, unreliable. To obtain a better calculation and to achieve better assignment, anharmonic corrections must be incorporated. At present we are in the process of developing a vibrational self-consistent field scheme that will overcome some of these difficulties. The lack of an unperturbed chromophore in these molecules requires the use of a broad spectral region for reliable identification of an explosive. This suggests that the utilization of spectroscopy-based remote detection based on narrow bands in this spectral region may not be very accurate or useful.

ACKNOWLEDGMENTS

Partial support for this research was obtained from NATO (SFP 980873). We thank Dr. B. Brauer for help in assignment of TATP frequencies.

1. N. A. Milas and A. Golubovic, J. Am. Chem. Soc. **81,** 6461 (1959).
2. A. Wierzbicki, E. A. Salter, E. A. Cioffi, and E. D. Stevens, J. Phys. Chem. A **105,** 8763 (2001).
3. J. C. Oxley, J. L. Smith, H. Chen, and E. Cioffi, Thermochimica Acta **388,** 215 (2002).
4. J. C. Oxley, J. L. Smith, and H. Chen, Propellants, Explos., Pyrotech. **27,** 209 (2002).
5. G. A. Buttigieg, A. K. Knight, S. Denson, C. Pommier, and M. B. Denton, Forensic Sci. Int. **135,** 53059 (2003).
6. F. Dubnikova, R. Kosloff, Y. Zeiri, and Z. Karpas, J. Phys. Chem. A **106,** 4951 (2002).
7. F. Dubnikova, R. Kosloff, J. Almog, Y. Zeiri, R. Boese, H. Izhaky, A. Alt, and E. Keinan, J. Am. Chem. Soc. **127,** 1146 (2005).
8. A. C. T. van Duin, Y. Zeiri, F. Dubnikova, R. Kosloff, and W. A. Goddard III, J. Am. Chem. Soc. **127,** 11053 (2005).
9. G. N. Eyler, J. Phys. Org. Chem. **19,** 776 (2006).
10. I. Cotte-Rodriguez, H. Chen, and R. G. Cooks, Chem. Commun. 953 (2006).
11. A. O. Terentèv, M. M. Platonov, E. J. Sonneveld, R. Peschar, V. V. Chernychev, Z. A. Starikova, and G. I. Nikishin, J. Org. Chem. **72,** 7237 (2007).
12. J. F. Federici, D. Gary, R. Barat, and D. Zimdars, Proc. SPIE-Int. Soc. Opt. Eng. **75,** 5781 (2005).
13. C. Schöllhorn, A. M. Fuller, J. Gratier, and R. E. Hummel, Appl. Opt. **46,** 6232 (2007).
14. R. E. Hummel, A. M. Fuller, C. Schöllhorn, and P. H. Holloway, Appl. Phys. Lett. **88,** 231903 (2006).
15. J. C. Carter, S. M. Angel, M. Lawrence-Snyder, J. Scaffidi, R. E. Whipple, and J. G. Reynolds, Appl. Spectrosc. **59,** 769 (2005).
16. T. Arusi-Parpar, D. Haflinger, Y. Ron, and R. Lavi, Opt. Commun. **204,** 327 (2002).
17. L. Pacheco-Londono, A. J. Pena, O. M. Primera, S. P. Hernandez-Rivera, N. Mina, R. Garcia, R. T. Chamberlain, and R. Lareau, Proc. SPIE-Int. Soc. Opt. Eng. **279,** 5403 (2004).
18. L. Pacheco-Londono, O. M. Primera, and S. Hernandez-Rivera, Proc. SPIE-Int. Soc. Opt. Eng. **190,** 5617 (2004).
19. M. J. Frisch, G. W. Trucks, H. B. Schlegel, G. E. Scuseria, M. A. Robb, J. R. Cheeseman, J. A. Montgomery, Jr., T. Vreven, K. N. Kudin, J. C. Burant, J. M. Millam, S. S. Iyengar, J. Tomasi, V. Barone, B. Mennucci, M. Cossi, G. Scalmani, N. Rega, G. A. Petersson, H. Nakatsuji, M. Hada, M. Ehara, K. Toyota, R. Fukuda, J. Hasegawa, M. Ishida, T. Nakajima, Y. Honda, O. Kitao, H. Nakai, M. Klene, X. Li, J. E. Knox, H. P. Hratchian, J. B. Cross, V. Bakken, C. Adamo, J. Jaramillo, R. Gomperts, R. E. Stratmann, O. Yazyev, A. J. Austin, R. Cammi, C. Pomelli, J. W. Ochterski, P. Y. Ayala, K. Morokuma, G. A. Voth, P. Salvador, J. J. Dannenberg, V. G. Zakrzewski, S. Dapprich, A. D. Daniels, M. C. Strain, O. Farkas, D. K. Malick, A. D. Rabuck, K. Raghavachari, J. B. Foresman, J. V. Ortiz, Q. Cui, A. G. Baboul, S. Clifford, J. Cioslowski, B. B. Stefanov, G. Liu, A. Liashenko, P. Piskorz, I. Komaromi, R. L. Martin, D. J. Fox, T. Keith, M. A. Al-Laham, C. Y. Peng, A. Nanayakkara, M. Challacombe, P. M. W. Gill, B. Johnson, W. Chen, M. W. Wong, C. Gonzalez, and J. A. Pople, *Gaussian 03*, Revision D.01 (Gaussian, Inc., Wallingford, CT, 2004).
20. T. H. Dunning, Jr., J. Chem. Phys. **90,** 1007 (1989).
21. M. W. Schmidt, K. K. Baldrige, J. K. Boatz, S. T. Elbert, M. S. Gordon, J. H. Jensen, S. Koseki, J. A. Matsunaga, K. A. Nguyen, S. J. Su, T. L. Windus, M. Dipuis, and J. A. Montgomery, J. Comput. Chem. **14,** 1347 (1993).
22. J. Kong, C. A. White, A. I. Krylov, C. D. Sherrill, R. D. Adamson, T. R. Furlani, M. S. Lee, A. M. Lee, S. R. Gwaltney, T. R. Adams, C. Ochsenfeld, A. T. B. Gilbert, G. S. Kedziora, V. A. Rassolov, D. R. Maurice, N. Nair, Y. Shao, N. A. Besley, P. E. Maslen, J. P. Dombroski, H. Daschel, W. Zhang, P. P. Korambath, J. Baker, E. F. C. Byrd, T. Van Voorhis, M. Oumi, S. Hirata, C.-P. Hsu, N. Ishikawa, J. Florian, A. Warshel, B. G. Johnson, P. M. W. Gill, M. Head-Gordon, and J. A. Pople, Comput. Chem. **21,** 1532 (2000).

23. C. Lee, W. Yang, and R. G. Parr, Phys. Rev. B **37,** 785 (1988).
24. F. A. Hamprecht, A. J. Cohen, D. J. Tozer, and N. C. Handy, J. Chem. Phys. **109,** 6264 (1998).
25. J.-O. Jung and R. B. Gerber, J. Chem. Phys. **105,** 10332 (1996).
26. B. Brauer, F. Dubnikova, Y. Zeiri, R. Kosloff, and R. B. Gerber, "Vibrational Spectroscopy of Triacetone Triperoxide (TATP): Anharmonic Fundamentals, Overtones and Combination Bands", Spectrochim. Acta, Part A, paper in press (2008).
27. J. A. Pople, H. B. Schlegel, R. Krishnan, D. J. Defrees, J. S. Blinkley, M. J. Frisch, R. A. Whiteside, R. F. Hout, and W. J. Hehre, Int. J. Quant. Chem. Symp. **15,** 269 (1981).
28. G. Rauhut and P. Pulay, J. Phys. Chem. **99,** 3093 (1995).
29. P. Sinha, S. E. Bosch, C. Gu, R. A. Wheeler, and A. K. Wilson, J. Phys. Chem. A **108,** 9213 (2004).
30. L. Radom and A. P. Scott, J. Phys. Chem. **100,** 16502 (1996).
31. S. D. McGrane, J. Barber, and J. Quenneville, J. Phys. Chem. A **109,** 9919 (2005).